Second harmonic generation of magnetic and dielectric multilayers

2006 J. Phys.: Condens. Matter 18 4329

(http://iopscience.iop.org/0953-8984/18/17/019)

INSTITUTE OF PHYSICS PUBLISHING JOURNAL OF PHYSICS: CONDENSED MATTER

J. Phys.: Condens. Matter **18** (2006) 4329–4343 doi:10.1088/0953-8984/18/17/019

Second harmonic generation of magnetic and dielectric multilayers

Siew-Choo Lim

School of Physics, Universiti Sains Malaysia, 11800 Minden, Penang, Malaysia

E-mail: limsiewchoo1@yahoo.com

Received 7 January 2006, in final form 27 March 2006
Published 13 April 2006
Online at stacks.iop.org/JPhysCM/18/4329

Abstract

The second harmonic generation of antiferromagnetic and dielectric multilayers is analysed by using a conventional nonlinear optics approach and transfer matrix formalism. The theoretical modelling of the multilayers is configured in Voigt geometry in order to observe second harmonic transmission and reflection through the film system, with the assumption of weak nonlinearity and no depletion of incident waves. With these, some of the linear and second harmonic transmissions and reflections are calculated numerically and shown graphically.

1. Introduction

Since the linear electromagnetic propagation and dielectric function of semiconductor and dielectric superlattices have been studied extensively and well understood [1–3], attention has been devoted to the study of linear effects of superlattices of other physical systems, such as magnetic/nonmagnetic superlattices [4–8]. These studies have been extended to the nonlinear regime, as shown in [9–12]. In order to study nonlinear effects in superlattices, two approaches have been used to simplify the complications due to the coupling of multilayer structures with nonlinearities. One of these is the effective medium approach for the analysis of dispersion properties of antiferromagnetic/nonmagnetic superlattices [12]. The other approach is the combination of Green-function analysis and transfer matrix technique for the optical harmonic generation of III–V compound GaP/AlP superlattices [10]. There are other approaches being used in studying the vast number of nonlinear phenomena in magnetic/nonmagnetic superlattices, for example the gap solitons [9], and electric polarization based magnetization induced second harmonic generation [11].

In this paper, the study is focused on the generation of second harmonic waves from antiferromagnetic/dielectric multilayers induced by incident intense far infrared electromagnetic field. This is an extension of the previous calculation on the generation of second harmonic waves from a simple uniaxial two-sublattice antiferromagnetic film (FeF_2) with weak nonlinearity [13, 14], within the conventional methods of nonlinear optics [15, 16]. In this paper, the approach being used in the analysis of linear and second harmonic

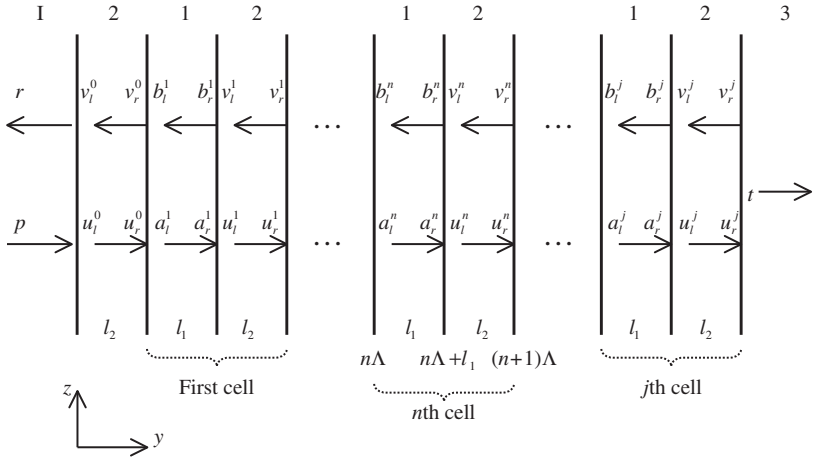

Figure 1. Schematic diagram for complex amplitudes of the magnetic field of the linear waves in the entire antiferromagnetic/dielectric multilayers.

transmission and reflection of antiferromagnetic/dielectric (FeF_2/ZnF_2) multilayers is entirely based on conventional nonlinear optics and the transfer matrix technique [1, 14]. The difference from the method adopted by Hashizume *et al* [10] is the assumption of weak nonlinearity with no depleted input waves; therefore, the Green-function analysis can be neglected and the calculation is simpler.

The paper is structured as follows. The theoretical modelling is shown in section 2, where four main derivations are given: transfer matrix formalism of linear waves in the multilayers, calculation of linear transmission and reflection coefficients through the multilayers, transfer matrix formalism of second harmonic waves in the multilayers, and calculation of second harmonic transmission and reflection through the multilayers. In section 3 the theoretical results, together with their implications, are presented graphically. Finally, conclusions are drawn in section 4.

2. Theoretical modelling

The main idea of the theoretical model is an extension of the previous calculations, where the propagation of linear and second harmonic waves in an FeF_2 film in Voigt geometry is calculated based on Maxwell's equations and conventional nonlinear optics approach with the assumption of weak nonlinearity and no depleted input waves [14]. Within this approach, the idea is extended to FeF_2/dielectric multilayers by using the transfer matrix technique [1]. The mathematical derivations are shown in the following subsections.

2.1. Transfer matrix formalism of linear waves in antiferromagnet/dielectric multilayers

The multilayers will be considered to be composed of antiferromagnetic (FeF_2) and dielectric (ZnF_2) slabs with thicknesses such that their macroscopic descriptions based on the corresponding magnetic susceptibilities and dielectric functions are perfectly adequate. A schematic diagram of the multilayer structure is shown in figure 1 to guide the derivations of the transfer matrix of the adjacent unit cells. The ZnF_2 and FeF_2 slabs are labelled as medium 1 and medium 2 respectively, with the corresponding thicknesses l_1 and l_2. As in the previous

calculations [14], the multilayers are configured in Voigt geometry, where both the easy axis of the antiferromagnetic slabs and the applied static magnetic field are in the direction of the z-axis or parallel to the plane of the slabs.

In Voigt geometry, as shown in figure 1, the intense far infrared electromagnetic field propagates along the y-axis and its magnetic component is along the x-axis. The linear wave equations induced in the slabs are derived from the Maxwell's equations and the appropriate constitutive relations. In medium 1 or dielectric slabs, the spatial part of the wave equation is

$$\frac{\partial^2 H_{x0}(y)}{\partial y^2} + k_1^2 H_{x0}(y) = 0 \tag{1}$$

where $k_1 = \omega(\varepsilon_0\varepsilon_1\mu_0)^{1/2}$ is the magnitude of the propagation vector in medium 1, and ω is the frequency of the incident waves. In medium 2 or FeF_2 slabs, the spatial part of the wave equation is

$$\frac{\partial^2 H_{x0}(y)}{\partial y^2} + k_{\mathrm{V}}^2 H_{x0}(y) = 0 \tag{2}$$

where $k_{\mathrm{V}} = \omega(\varepsilon_0\varepsilon_2\mu_0\mu_{\mathrm{V}})^{1/2}$ is the magnitude of the propagation vector in medium 2, and $\mu_{\mathrm{V}} = \mu_{xx} + \frac{(\mu_{xy})^2}{\mu_{xx}}$ is the Voigt permeability [13, 14]. Based on equation (1), the general solutions for the linear magnetic and electric fields in medium 1 in the nth cell are

$$H_{1x}^n(y,t) = \tfrac{1}{2}\left[a_l^n \exp[\mathrm{i}k_1(y - n\Lambda)] + b_l^n \exp[-\mathrm{i}k_1(y - n\Lambda)]\right]\exp(-\mathrm{i}\omega t) + \text{c.c.} \tag{3}$$

or

$$H_{1x}^n(y,t) = \tfrac{1}{2}\left[a_r^n \exp[\mathrm{i}k_1(y - n\Lambda - l_1)] + b_r^n \exp[-\mathrm{i}k_1(y - n\Lambda - l_1)]\right]\exp(-\mathrm{i}\omega t) + \text{c.c.} \tag{4}$$

and

$$E_{1z}^n(y,t) = \frac{1}{2}\frac{q_1}{\varepsilon_0\omega}\left[a_l^n \exp[\mathrm{i}k_1(y - n\Lambda)] - b_l^n \exp[-\mathrm{i}k_1(y - n\Lambda)]\right]\exp(-\mathrm{i}\omega t) + \text{c.c.} \tag{5}$$

or

$$E_{1z}^n(y,t) = \frac{1}{2}\frac{q_1}{\varepsilon_0\omega}\left[a_r^n \exp[\mathrm{i}k_1(y - n\Lambda - l_1)] - b_r^n \exp[-ik_1(y - n\Lambda - l_1)]\right] \times \exp(-\mathrm{i}\omega t) + \text{c.c.} \tag{6}$$

where $q_1 = k_1/\varepsilon_1$ and a_l^n and b_l^n are the complex amplitudes of the magnetic field travelling in the positive and negative y-directions respectively. The subscripts l and r represent the positions of the coefficients immediately to the left and to the right of an interface. Based on equation (2), the general solutions for the linear magnetic and electric fields in medium 2 (FeF_2) in the nth cell are

$$H_{2x}^n(y,t) = \tfrac{1}{2}\left[u_l^n \exp[\mathrm{i}k_{\mathrm{V}}(y - n\Lambda - l_1)] + v_l^n \exp[-\mathrm{i}k_{\mathrm{V}}(y - n\Lambda - l_1)]\right]\exp(-\mathrm{i}\omega t) + \text{c.c.} \tag{7}$$

or

$$H_{2x}^n(y,t) = \tfrac{1}{2}\left[u_r^n \exp[\mathrm{i}k_{\mathrm{V}}(y - (n+1)\Lambda)] + v_r^n \exp[-\mathrm{i}k_{\mathrm{V}}(y - (n+1)\Lambda)]\right] \times \exp(-\mathrm{i}\omega t) + \text{c.c.} \tag{8}$$

and

$$E_{2z}^n(y,t) = \frac{1}{2}\frac{q_{\mathrm{V}}}{\varepsilon_0\omega}\left[u_l^n \exp[\mathrm{i}k_{\mathrm{V}}(y - n\Lambda - l_1)] - v_l^n \exp[-\mathrm{i}k_{\mathrm{V}}(y - n\Lambda - l_1)]\right] \times \exp(-\mathrm{i}\omega t) + \text{c.c.} \tag{9}$$

or

$$E_{2z}^{n}(y,t) = \frac{1}{2}\frac{q_{\mathrm{V}}}{\varepsilon_0\omega}\left[u_r^n \exp[\mathrm{i}k_{\mathrm{V}}(y-(n+1)\Lambda)] - v_r^n \exp[-\mathrm{i}k_{\mathrm{V}}(y-(n+1)\Lambda)]\right] \times \exp[-\mathrm{i}\omega t] + \text{c.c.} \tag{10}$$

where $q_{\mathrm{V}} = k_{\mathrm{V}}/\varepsilon_2$ and, u_l^n and v_l^n are the complex amplitudes of the magnetic field travelling in the positive and negative y-directions respectively. The complex amplitudes of magnetic fields of the same medium can be related by appropriate phase factors, which can be rewritten as matrices. In medium 1, these are

$$\begin{pmatrix} a_l^n \\ b_l^n \end{pmatrix} = \mathbf{T_1}\begin{pmatrix} a_r^n \\ b_r^n \end{pmatrix} \qquad \text{or} \qquad \begin{pmatrix} a_r^n \\ b_r^n \end{pmatrix} = \mathbf{T_2}\begin{pmatrix} a_l^n \\ b_l^n \end{pmatrix} \tag{11}$$

where

$$\mathbf{T_1} = \begin{pmatrix} \exp(-\mathrm{i}k_1 l_1) & 0 \\ 0 & \exp(\mathrm{i}k_1 l_1) \end{pmatrix} \qquad \text{and}$$

$$\mathbf{T_2} = (\mathbf{T_1})^{-1} = \begin{pmatrix} \exp(\mathrm{i}k_1 l_1) & 0 \\ 0 & \exp(-\mathrm{i}k_1 l_1) \end{pmatrix}. \tag{12}$$

In medium 2, the complex amplitudes are related as

$$\begin{pmatrix} u_l^n \\ v_l^n \end{pmatrix} = \mathbf{T_3}\begin{pmatrix} u_r^n \\ v_r^n \end{pmatrix} \qquad \text{or} \qquad \begin{pmatrix} u_r^n \\ v_r^n \end{pmatrix} = \mathbf{T_4}\begin{pmatrix} u_l^n \\ v_l^n \end{pmatrix} \tag{13a}$$

where

$$\mathbf{T_3} = \begin{pmatrix} \exp(-\mathrm{i}k_{\mathrm{V}} l_2) & 0 \\ 0 & \exp(\mathrm{i}k_{\mathrm{V}} l_2) \end{pmatrix} \qquad \text{and}$$

$$\mathbf{T_4} = (\mathbf{T_3})^{-1} = \begin{pmatrix} \exp(\mathrm{i}k_{\mathrm{V}} l_2) & 0 \\ 0 & \exp(-\mathrm{i}k_{\mathrm{V}} l_2) \end{pmatrix}. \tag{13b}$$

Based on equations (3)–(6) and (7)–(10), and applying the standard boundary conditions for magnetic and electric fields on $y = n\Lambda + l_1$ and $y = (n+1)\Lambda$ interfaces, we have four boundary equations:

$$a_r^n + b_r^n = u_l^n + v_l^n \tag{14a}$$

$$q_1\left(a_r^n - b_r^n\right) = q_{\mathrm{V}}\left(u_l^n - v_l^n\right) \tag{14b}$$

$$u_r^n + v_r^n = a_l^{n+1} + b_l^{n+1} \tag{14c}$$

$$q_{\mathrm{V}}\left(u_r^n - v_r^n\right) = q_1\left(a_l^{n+1} - b_l^{n+1}\right). \tag{14d}$$

From these boundary equations, the complex amplitudes across medium 1 and medium 2 are related as

$$\begin{pmatrix} u_l^n \\ v_l^n \end{pmatrix} = \mathbf{T_5}\begin{pmatrix} a_r^n \\ b_r^n \end{pmatrix} \qquad \text{or} \qquad \begin{pmatrix} a_r^n \\ b_r^n \end{pmatrix} = \mathbf{T_6}\begin{pmatrix} u_l^n \\ v_l^n \end{pmatrix} \tag{15a}$$

$$\begin{pmatrix} u_r^n \\ v_r^n \end{pmatrix} = \mathbf{T_5}\begin{pmatrix} a_l^{n+1} \\ b_l^{n+1} \end{pmatrix} \qquad \text{or} \qquad \begin{pmatrix} a_l^{n+1} \\ b_l^{n+1} \end{pmatrix} = \mathbf{T_6}\begin{pmatrix} u_r^n \\ v_r^n \end{pmatrix} \tag{15b}$$

where

$$\mathbf{T_5} = \frac{1}{2}\begin{pmatrix} 1+\frac{q_1}{q_{\mathrm{V}}} & 1-\frac{q_1}{q_{\mathrm{V}}} \\ 1-\frac{q_1}{q_{\mathrm{V}}} & 1+\frac{q_1}{q_{\mathrm{V}}} \end{pmatrix} \qquad \text{and} \qquad \mathbf{T_6} = (\mathbf{T_5})^{-1} = \frac{1}{2}\begin{pmatrix} 1+\frac{q_{\mathrm{V}}}{q_1} & 1-\frac{q_{\mathrm{V}}}{q_1} \\ 1-\frac{q_{\mathrm{V}}}{q_1} & 1+\frac{q_{\mathrm{V}}}{q_1} \end{pmatrix}. \tag{15c}$$

From equations (15), the complex amplitudes in the adjacent unit cells are related as

$$\begin{pmatrix} a_l^{n+1} \\ b_l^{n+1} \end{pmatrix} = \mathbf{\Pi}\begin{pmatrix} a_l^n \\ b_l^n \end{pmatrix} \tag{16a}$$

where

$$\mathbf{\Pi} = \mathbf{T_6 T_4 T_5 T_2} \tag{16b}$$

is the transfer matrix across one unit cell of the linear waves.

2.2. Calculation of linear transmission and reflection coefficients through antiferromagnetic/dielectric multilayers

Based on the linear transfer matrix in equations (16*a*) and (16*b*), and the schematic diagram in figure 1, the linear wave transmission and reflection coefficients of the entire antiferromagnetic/dielectric multilayer are derived as follows. As in section 2.1, the linear wave equations in the incident medium I and substrate medium 3 are derived from the Maxwell's equations and the appropriate constitutive relations. In medium I, the spatial part of the wave equation is

$$\frac{\partial^2 H_{x0}(y)}{\partial y^2} + k_{\mathrm{I}}^2 H_{x0}(y) = 0 \tag{17}$$

where $k_{\mathrm{I}} = \omega\sqrt{\varepsilon_0\mu_0\varepsilon_{\mathrm{I}}}$ is the magnitude of the propagation vector in medium I, and ε_{I} is the dielectric constants for medium I. In medium 3,

$$\frac{\partial^2 H_{x0}(y)}{\partial y^2} + k_3^2 H_{x0}(y) = 0 \tag{18}$$

$k_3 = \omega\sqrt{\varepsilon_0\mu_0\varepsilon_3}$ is the magnitude of the propagation vector in medium 3, and ε_3 is the dielectric constants for medium 3. Based on equations (17) and (18), the general solutions of linear magnetic and electric fields in medium I and medium 3 are

$$H_{\mathrm{I}x}(y,t) = \tfrac{1}{2}\left[p\exp(\mathrm{i}k_{\mathrm{I}}y) + r\exp(-\mathrm{i}k_{\mathrm{I}}y)\right]\exp(-\mathrm{i}\omega t) + \text{c.c.} \tag{19}$$

$$E_{I z}(y,t) = \frac{1}{2}\frac{q_{\mathrm{I}}}{\varepsilon_0\omega}\left[p\exp(\mathrm{i}k_{\mathrm{I}}y) - r\exp(-\mathrm{i}k_{\mathrm{I}}y)\right]\exp(-\mathrm{i}\omega t) + \text{c.c.} \tag{20}$$

$$H_{3x}(y,t) = \tfrac{1}{2}t\exp[\mathrm{i}k_3(y - j\Lambda - l_2)]\exp(-\mathrm{i}\omega t) + \text{c.c.} \tag{21}$$

$$E_{3z}(y,t) = \frac{1}{2}\frac{q_3}{\varepsilon_0\omega}t\exp[\mathrm{i}k_3(y - j\Lambda - l_2)]\exp(-\mathrm{i}\omega t) + \text{c.c.} \tag{22}$$

where $q_{\mathrm{I}} = k_{\mathrm{I}}/\varepsilon_{\mathrm{I}}$ and $q_3 = k_3/\varepsilon_3$.

Based on equation (2), the magnetic and electric fields of the left interface in medium 2 of the zeroth cell are

$$H_{2x}^0(y,t) = \tfrac{1}{2}\left[u_l^0\exp(\mathrm{i}k_{\mathrm{V}}y) + v_l^0\exp(-\mathrm{i}k_{\mathrm{V}}y)\right]\exp(-\mathrm{i}\omega t) + \text{c.c.} \tag{23}$$

$$E_{2z}^0(y,t) = \frac{1}{2}\frac{q_{\mathrm{V}}}{\varepsilon_0\omega}\left[u_l^0\exp(\mathrm{i}k_{\mathrm{V}}y) - v_l^0\exp(-\mathrm{i}k_{\mathrm{V}}y)\right]\exp(-\mathrm{i}\omega t) + \text{c.c.} \tag{24}$$

and the magnetic and electric fields of the right interface in medium 2 of the jth cell are

$$H_{2x}^j(y,t) = \tfrac{1}{2}\left[u_r^j\exp[\mathrm{i}k_{\mathrm{V}}(y - j\Lambda - l_2)] + v_r^j\exp[-\mathrm{i}k_{\mathrm{V}}(y - j\Lambda - l_2)]\right] \times \exp(-\mathrm{i}\omega t) + \text{c.c.} \tag{25}$$

$$E_{2z}^j(y,t) = \frac{1}{2}\frac{q_{\mathrm{V}}}{\varepsilon_0\omega}\left[u_r^j\exp[\mathrm{i}k_{\mathrm{V}}(y - j\Lambda - l_2)] - v_r^j\exp[-\mathrm{i}k_{\mathrm{V}}(y - j\Lambda - l_2)]\right] \times \exp(-\mathrm{i}\omega t) + \text{c.c.} \tag{26}$$

Applying boundary conditions at the $y = 0$ interface for the equation pairs (19) and (23), (20) and (24), and at the $y = j\Lambda + l_2$ interface for equation pairs (21) and (25), (22) and (26),

we have four boundary equations, relating the outside complex amplitudes to the complex amplitudes immediately inside the multilayer:

$$p + r = u_l^0 + v_l^0 \tag{27a}$$

$$q_{\mathrm{I}} p - q_{\mathrm{I}} r = q_{\mathrm{V}} u_l^0 - q_{\mathrm{V}} v_l^0 \tag{27b}$$

$$u_r^j + v_r^j = t \tag{27c}$$

$$q_{\mathrm{V}} u_r^j - q_{\mathrm{V}} v_r^j = q_3 t. \tag{27d}$$

Inside the multilayers, the complex amplitudes in medium 2 of the zeroth and jth unit cells are related by using the linear transfer matrix equations (16*a*) and (16*b*). The result is

$$\begin{pmatrix} u_r^j \\ v_r^j \end{pmatrix} = \boldsymbol{\Theta} \begin{pmatrix} u_l^0 \\ v_l^0 \end{pmatrix} \qquad \text{or} \qquad \begin{aligned} u_r^j &= \Theta_{11} u_l^0 + \Theta_{12} v_l^0 \\ v_r^j &= \Theta_{21} u_l^0 + \Theta_{22} v_l^0 \end{aligned} \tag{28a}$$

where

$$\boldsymbol{\Theta} = \mathbf{T_4 T_5 T_2} \left(\boldsymbol{\Pi}\right)^{j-1} \mathbf{T}_6 \mathbf{T}_4. \tag{28b}$$

Substituting equation (28*a*) into the four boundary equations (27*c*)–(27*d*), the solutions of the linear transmission and reflection coefficients are obtained:

$$r = u_l^0 + v_l^0 - p \tag{29a}$$

$$t = \left(\Theta_{11} + \Theta_{21}\right) u_l^0 + \left(\Theta_{12} + \Theta_{22}\right) v_l^0 \tag{29b}$$

where

$$u_l^0 = \frac{2 q_{\mathrm{I}} p \left\{q_{\mathrm{V}} \left(\Theta_{12} - \Theta_{22}\right) - q_3 \left(\Theta_{12} + \Theta_{22}\right)\right\}}{\left(q_{\mathrm{I}} + q_{\mathrm{V}}\right) \left\{q_{\mathrm{V}} \left(\Theta_{12} - \Theta_{22}\right) - q_3 \left(\Theta_{12} + \Theta_{22}\right)\right\} - \left(q_{\mathrm{I}} - q_{\mathrm{V}}\right) \left\{q_{\mathrm{V}} \left(\Theta_{11} - \Theta_{21}\right) - q_3 \left(\Theta_{11} + \Theta_{21}\right)\right\}} \tag{29c}$$

$$v_l^0 = \frac{-2 q_{\mathrm{I}} p \left\{q_{\mathrm{V}} \left(\Theta_{11} - \Theta_{21}\right) - q_3 \left(\Theta_{11} + \Theta_{21}\right)\right\}}{\left(q_{\mathrm{I}} + q_{\mathrm{V}}\right) \left\{q_{\mathrm{V}} \left(\Theta_{12} - \Theta_{22}\right) - q_3 \left(\Theta_{12} + \Theta_{22}\right)\right\} - \left(q_{\mathrm{I}} - q_{\mathrm{V}}\right) \left\{q_{\mathrm{V}} \left(\Theta_{11} - \Theta_{21}\right) - q_3 \left(\Theta_{11} + \Theta_{21}\right)\right\}}. \tag{29d}$$

Calculations of Poynting's vector in medium I and medium 3 show that the linear transmission ($\equiv T$) and reflection coefficients ($\equiv R$) through the entire multilayers are

$$T = \frac{\varepsilon_{\mathrm{I}}}{\varepsilon_3} \frac{|t|^2}{|p|^2} \qquad \text{and} \qquad R = \frac{|r|^2}{|p|^2} \tag{30}$$

where p is the amplitude of input waves, and $|p|^2$ is directly proportional to the input power I_p as

$$I_p = \frac{1}{2} \frac{k_{\mathrm{I}}}{\varepsilon_0 \varepsilon_{\mathrm{I}} \omega} |p|^2 . \tag{31}$$

2.3. Transfer matrix formalism of second harmonic waves in antiferromagnetic/dielectric multilayers

The transfer matrix formalism of the second harmonic waves across the slabs is similar to the linear waves. Compared to the linear wave equation, the basic difference is due to an additional source term. The source is in terms of the linear complex amplitudes. The solution of these inhomogeneous second order differential equations carry the source in their particular solutions, and result in the fields in antiferromagnetic slabs. To assist the derivation, a schematic diagram for complex amplitudes of the magnetic field of the linear and second harmonic waves in the entire antiferromagnetic/dielectric multilayers is sketched in figure 2.

In Voigt geometry, for an incident dynamic wave with its magnetic component along the x-axis, the induced second harmonic waves in medium 2 have magnetic component along the

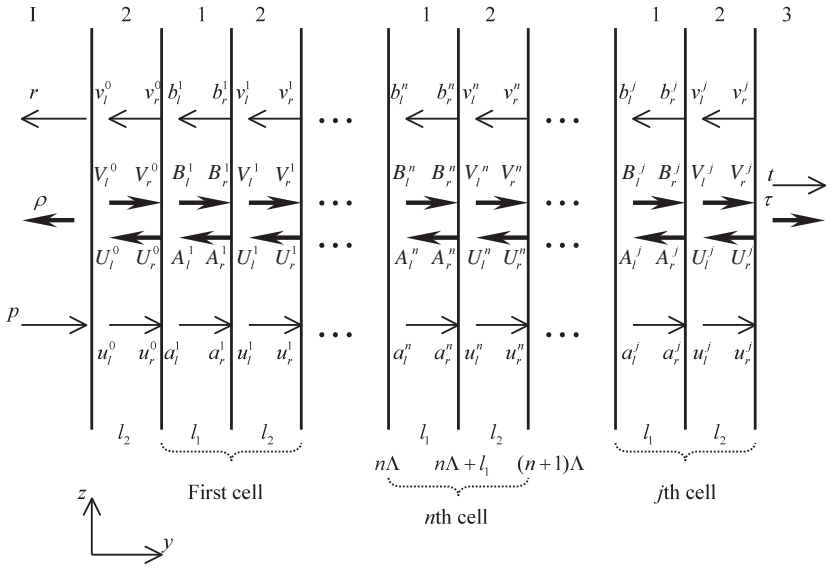

Figure 2. Schematic diagram for complex amplitudes of the magnetic field of the linear (thin arrows) and second harmonic (thick arrows) waves in the entire antiferromagnetic/dielectric multilayers

z-axis, due to nonzero susceptibility tensor elements χ_{zxx} and χ_{zyy} [13, 14]. The spatial part of the second harmonic wave equations induced in medium 1 is

$$\frac{\partial^2 H_{z0}(y)}{\partial y^2} + \alpha_1^2 H_{z0}(y) = 0 \tag{32}$$

where $\alpha_1^2 = \Omega^2 \varepsilon_0 \varepsilon_1 \mu_0$, and ε_1 is evaluated at second harmonic frequency, $\Omega = 2\omega$, but usually ε_1 (dielectric) is considered frequency independent. In medium 2,

$$\frac{\partial^2 H_{z0}(y)}{\partial y^2} + \alpha_2^2 H_{z0}(y) = \Gamma H_{x0}(y) H_{x0}(y) \tag{33}$$

where $\alpha_2^2 = \Omega^2 \varepsilon_0 \varepsilon_2 \mu_0$, and $\Gamma = -\frac{1}{2}\chi_{zxx}[1 + (\frac{\mu_{xy}}{\mu_{xx}})^2]$ as in [14], is the source of the second harmonic waves. ε_2 is evaluated at Ω, but Γ is evaluated at ω. By using equation (32), the general solutions of the magnetic and electric fields in medium 1 of the nth cell are

$$H_{1z}^n = \tfrac{1}{2}\left[A_l^n \exp[\mathrm{i}\alpha_1(y - n\Lambda)] + B_l^n \exp[-\mathrm{i}\alpha_1(y - n\Lambda)]\right]\exp(-\mathrm{i}\Omega t) + \text{c.c.} \tag{34}$$

or

$$H_{1z}^n = \tfrac{1}{2}\left[A_r^n \exp[\mathrm{i}\alpha_1(y - n\Lambda - l_1)] + B_r^n \exp[-\mathrm{i}\alpha_1(y - n\Lambda - l_1)]\right]\exp(-\mathrm{i}\Omega t) + \text{c.c.} \tag{35}$$

and

$$E_{1x}^n = \frac{1}{2}\frac{Q_1}{\varepsilon_0 \Omega}\left[-A_l^n \exp[\mathrm{i}\alpha_1(y - n\Lambda)] + B_l^n \exp[-\mathrm{i}\alpha_1(y - n\Lambda)]\right]\exp(-\mathrm{i}\Omega t) + \text{c.c.} \tag{36}$$

or

$$E_{1x}^n = \frac{1}{2}\frac{Q_1}{\varepsilon_0 \Omega}\left[-A_r^n \exp[\mathrm{i}\alpha_1(y - n\Lambda - l_1)] + B_r^n \exp[-\mathrm{i}\alpha_1(y - n\Lambda - l_1)]\right] \times \exp(-\mathrm{i}\Omega t) + \text{c.c.} \tag{37}$$

where $Q_1 = \alpha_1/\varepsilon_1$. By using equation (33), the magnetic and electric fields in medium 2 (magnetic medium) of the nth cell are

$$H_{2z}^n = \tfrac{1}{2}\big[U_l^n \exp[\mathrm{i}\alpha_2(y - n\Lambda - l_1)] + V_l^n \exp[-\mathrm{i}\alpha_2(y - n\Lambda - l_1)] + f_{1l}^n \exp[\mathrm{i}\xi(y - n\Lambda - l_1)] + f_{2l}^n \exp[-\mathrm{i}\xi(y - n\Lambda - l_1)] + f_{3l}^n\big] \times \exp(-\mathrm{i}\Omega t) + \text{c.c.} \tag{38}$$

or

$$H_{2z}^n = \tfrac{1}{2}\big[U_r^n \exp\big\{\mathrm{i}\alpha_2\big[y - (n+1)\Lambda\big]\big\} + V_r^n \exp\big\{-\mathrm{i}\alpha_2\big[y - (n+1)\Lambda\big]\big\} + f_{1r}^n \exp\big\{\mathrm{i}\xi\big[y - (n+1)\Lambda\big]\big\} + f_{2r}^n \exp\big\{-\mathrm{i}\xi\big[y - (n+1)\Lambda\big]\big\} + f_{3r}^n\big] \times \exp(-\mathrm{i}\Omega t) + \text{c.c.} \tag{39}$$

and

$$E_{2x}^n = \frac{1}{2}\frac{Q_2}{\varepsilon_0\Omega}\big[-U_l^n \exp[\mathrm{i}\alpha_2(y - n\Lambda - l_1)] + V_l^n \exp[-\mathrm{i}\alpha_2(y - n\Lambda - l_1)]\big]\exp(-\mathrm{i}\Omega t) + \frac{1}{2}\frac{Q_\mathrm{V}}{\varepsilon_0\Omega}\big[-f_{1l}^n \exp[\mathrm{i}\xi(y - n\Lambda - l_1)] + f_{2l}^n \exp[-\mathrm{i}\xi(y - n\Lambda - l_1)]\big] \times \exp(-\mathrm{i}\Omega t) + \text{c.c.} \tag{40}$$

or

$$E_{2x}^n = \frac{1}{2}\frac{Q_2}{\varepsilon_0\Omega}\big[-U_r^n \exp\{\mathrm{i}\alpha_2[y - (n+1)\Lambda]\} + V_r^n \exp\{-\mathrm{i}\alpha_2[y - (n+1)\Lambda]\}\big]\exp(-\mathrm{i}\Omega t) + \frac{1}{2}\frac{Q_\mathrm{V}}{\varepsilon_0\Omega}\big[-f_{1r}^n \exp\big\{\mathrm{i}\xi\big[y - (n+1)\Lambda\big]\big\} + f_{2r}^n \exp\big\{-\mathrm{i}\xi\big[y - (n+1)\Lambda\big]\big\}\big] \times \exp(-\mathrm{i}\Omega t) + \text{c.c.} \tag{41}$$

where $Q_2 = \alpha_2/\varepsilon_2$, $\xi = 2k_\mathrm{V}$, $Q_\mathrm{V} = \xi/\varepsilon_2$, and k_V is evaluated at ω. The sources in equations (38)–(41) are in terms of linear amplitudes. These are shown in equations (42a)–(42f):

$$f_{1l}^n = \left(u_l^n\right)^2 \Gamma/\left(\alpha_2^2 - \xi^2\right) \tag{42a}$$

$$f_{2l}^n = \left(v_l^n\right)^2 \Gamma/\left(\alpha_2^2 - \xi^2\right) \tag{42b}$$

$$f_{3l}^n = 2u_l^n v_l^n \Gamma/\alpha_2^2 \tag{42c}$$

and

$$f_{1r}^n = \left(u_r^n\right)^2 = \mathrm{e}^{\mathrm{i}2k_\mathrm{V}l_2}\left(u_l^n\right)^2 \Gamma/\left(\alpha_2^2 - \xi^2\right) \tag{42d}$$

$$f_{2r}^n = \left(v_r^n\right)^2 = \mathrm{e}^{-\mathrm{i}2k_\mathrm{V}l_2}\left(v_l^n\right)^2 \Gamma/\left(\alpha_2^2 - \xi^2\right) \tag{42e}$$

$$f_{3r}^n = 2u_r^n v_r^n = 2u_l^n v_l^n \Gamma/\alpha_2^2. \tag{42f}$$

The second harmonic magnetic and electric fields of the same medium can be related by an appropriate phase factor. For medium 1, from equations (34) to (37), these are

$$\begin{pmatrix} A_l^n \\ B_l^n \end{pmatrix} = \Phi_1 \begin{pmatrix} A_r^n \\ B_r^n \end{pmatrix} \qquad \text{or} \qquad \begin{pmatrix} A_r^n \\ B_r^n \end{pmatrix} = \Phi_2 \begin{pmatrix} A_l^n \\ B_l^n \end{pmatrix} \tag{43a}$$

where

$$\Phi_1 = \begin{pmatrix} \exp(-\mathrm{i}\alpha_1 l_1) & 0 \\ 0 & \exp(\mathrm{i}\alpha_1 l_1) \end{pmatrix} \qquad \text{and}$$

$$\Phi_2 = (\Phi_1)^{-1} = \begin{pmatrix} \exp(\mathrm{i}\alpha_1 l_1) & 0 \\ 0 & \exp(-\mathrm{i}\alpha_1 l_1) \end{pmatrix}. \tag{43b}$$

For medium 2, from equations (38) to (41), these are

$$\begin{pmatrix} U_l^n \\ V_l^n \end{pmatrix} = \Phi_3 \begin{pmatrix} U_r^n \\ V_r^n \end{pmatrix} \qquad \text{or} \qquad \begin{pmatrix} U_r^n \\ V_r^n \end{pmatrix} = \Phi_4 \begin{pmatrix} U_l^n \\ V_l^n \end{pmatrix} \tag{44a}$$

where

$$\Phi_3 = \begin{pmatrix} \exp(-\mathrm{i}\alpha_2 l_2) & 0 \\ 0 & \exp(\mathrm{i}\alpha_2 l_2) \end{pmatrix} \qquad \text{and}$$

$$\Phi_4 = (\Phi_3)^{-1} = \begin{pmatrix} \exp(\mathrm{i}\alpha_2 l_2) & 0 \\ 0 & \exp(-\mathrm{i}\alpha_2 l_2) \end{pmatrix}. \tag{44b}$$

Applying standard boundary conditions for the magnetic and electric fields at the $y = n\Lambda + l_1$ and $y = (n+1)\Lambda$ interfaces by referring to equations (34)–(41), we have four boundary equations for second harmonic complex amplitudes

$$A_r^n + B_r^n = U_l^n + V_l^n + \phi_{hl}^n \tag{45a}$$

$$Q_1\left(-A_r^n + B_r^n\right) = Q_2\left(-U_l^n + V_l^n\right) + \phi_{el}^n \tag{45b}$$

$$U_r^n + V_r^n + \phi_{hr}^n = A_l^{n+1} + B_l^{n+1} \tag{45c}$$

$$Q_2\left(-U_r^n + V_r^n\right) + \phi_{er}^n = Q_1\left(-A_l^{n+1} + B_l^{n+1}\right) \tag{45d}$$

where

$$\phi_{hl}^n = f_{1l}^n + f_{2l}^n + f_{3l}^n, \qquad \phi_{el}^n = Q_{\mathrm{V}}\left(-f_{1l}^n + f_{2l}^n\right) \tag{45e}$$

and

$$\phi_{hr}^n = f_{1r}^n + f_{2r}^n + f_{3r}^n, \qquad \phi_{er}^n = Q_{\mathrm{V}}\left(-f_{1r}^n + f_{2r}^n\right). \tag{45f}$$

The solutions of these boundary equations are

$$\begin{pmatrix} A_r^n \\ B_r^n \end{pmatrix} = \Phi_7 \begin{pmatrix} U_l^n \\ V_l^n \end{pmatrix} + \Phi_8^n \qquad \text{or} \qquad \begin{pmatrix} U_l^n \\ V_l^n \end{pmatrix} = \Phi_9 \begin{pmatrix} A_r^n \\ B_r^n \end{pmatrix} + \Phi_{10}^n \tag{46}$$

and

$$\begin{pmatrix} A_l^{n+1} \\ B_l^{n+1} \end{pmatrix} = \Phi_{11} \begin{pmatrix} U_r^n \\ V_r^n \end{pmatrix} + \Phi_{12}^n \qquad \text{or} \qquad \begin{pmatrix} U_r^n \\ V_r^n \end{pmatrix} = \Phi_{13} \begin{pmatrix} A_l^{n+1} \\ B_l^{n+1} \end{pmatrix} + \Phi_{14}^n \tag{47}$$

where

$$\Phi_7 = \begin{pmatrix} \frac{1}{2}(1+\frac{Q_2}{Q_1}) & \frac{1}{2}(1-\frac{Q_2}{Q_1}) \\ \frac{1}{2}(1-\frac{Q_2}{Q_1}) & \frac{1}{2}(1+\frac{Q_2}{Q_1}) \end{pmatrix}, \qquad \Phi_8^n = \begin{pmatrix} \frac{1}{2}(\phi_{hl}^n - \frac{1}{Q_1}\phi_{el}^n) \\ \frac{1}{2}(\phi_{hl}^n + \frac{1}{Q_1}\phi_{el}^n) \end{pmatrix} \tag{48}$$

$$\Phi_9 = \begin{pmatrix} \frac{1}{2}(1+\frac{Q_1}{Q_2}) & \frac{1}{2}(1-\frac{Q_1}{Q_2}) \\ \frac{1}{2}(1-\frac{Q_1}{Q_2}) & \frac{1}{2}(1+\frac{Q_1}{Q_2}) \end{pmatrix}, \qquad \Phi_{10}^n = \begin{pmatrix} \frac{1}{2}(\frac{1}{Q_2}\phi_{el}^n - \phi_{hl}^n) \\ -\frac{1}{2}(\frac{1}{Q_2}\phi_{el}^n + \phi_{hl}^n) \end{pmatrix} \tag{49}$$

$$\Phi_{11} = \Phi_7 = \begin{pmatrix} \frac{1}{2}(1+\frac{Q_2}{Q_1}) & \frac{1}{2}(1-\frac{Q_2}{Q_1}) \\ \frac{1}{2}(1-\frac{Q_2}{Q_1}) & \frac{1}{2}(1+\frac{Q_2}{Q_1}) \end{pmatrix}, \qquad \Phi_{12}^n = \begin{pmatrix} \frac{1}{2}(\phi_{hr}^n - \frac{1}{Q_1}\phi_{er}^n) \\ \frac{1}{2}(\phi_{hr}^n + \frac{1}{Q_1}\phi_{er}^n) \end{pmatrix} \tag{50}$$

$$\Phi_{13} = \Phi_9 = \begin{pmatrix} \frac{1}{2}(1+\frac{Q_1}{Q_2}) & \frac{1}{2}(1-\frac{Q_1}{Q_2}) \\ \frac{1}{2}(1-\frac{Q_1}{Q_2}) & \frac{1}{2}(1+\frac{Q_1}{Q_2}) \end{pmatrix}, \qquad \Phi_{14}^n = \begin{pmatrix} \frac{1}{2}(\frac{1}{Q_2}\phi_{er}^n - \phi_{hr}^n) \\ -\frac{1}{2}(\frac{1}{Q_2}\phi_{er}^n + \phi_{hr}^n) \end{pmatrix}. \tag{51}$$

Based on equations (46) and (47), the transfer matrix relates the second harmonic waves in adjacent unit cells as

$$\begin{pmatrix} A_l^{n+1} \\ B_l^{n+1} \end{pmatrix} = \Delta \begin{pmatrix} A_l^n \\ B_l^n \end{pmatrix} + \Upsilon^n \tag{52a}$$

where

$$\Delta = \Phi_{11}\Phi_4\Phi_9\Phi_2, \qquad \Upsilon^n = \Phi_{11}\Phi_4\Phi_{10}^n + \Phi_{12}^n. \tag{52b}$$

From equations (52*a*) and (52*b*), the second harmonic waves in the first cell and the nth cell are related as follows:

$$\begin{pmatrix} A_l^n \\ B_l^n \end{pmatrix} = (\Delta)^{n-1} \begin{pmatrix} A_l^1 \\ B_l^1 \end{pmatrix} + \sum_{r=1}^{n-1} (\Delta)^{n-1-r} \Upsilon^r. \tag{53}$$

2.4. Calculation of second harmonic transmission and reflection through antiferromagnetic/dielectric multilayers

The second harmonic transmission and reflection coefficients are derived based on the schematic diagram in figure 2 and the second harmonic transfer matrix shown in equations (52*a*)–(53). The methodology is the same as the calculation for the linear waves. The spatial part of the second harmonic wave equations induced in medium I is

$$\frac{\partial^2 H_{z0}(y)}{\partial y^2} + \alpha_{\mathrm{I}}^2 H_{z0}(y) = 0 \tag{54}$$

where $\alpha_{\mathrm{I}}^2 = \Omega^2 \varepsilon_0 \varepsilon_{\mathrm{I}} \mu_0$. In medium 3 this is

$$\frac{\partial^2 H_{z0}(y)}{\partial y^2} + \alpha_3^2 H_{z0}(y) = 0 \tag{55}$$

where $\alpha_3^2 = \Omega^2 \varepsilon_0 \varepsilon_3 \mu_0$. The general solutions of equations (54) and (55) give the second harmonic magnetic and electric fields in medium I and medium 3, respectively. These are

$$H_{Iz} = \tfrac{1}{2}\rho \exp(-\mathrm{i}\alpha_{\mathrm{I}} y) \exp(-\mathrm{i}\Omega t) + \text{c.c.} \tag{56}$$

$$E_{\mathrm{I}x} = \frac{1}{2}\frac{Q_{\mathrm{I}}}{\varepsilon_0 \Omega} \rho \exp(-\mathrm{i}\alpha_{\mathrm{I}} y) \exp(-\mathrm{i}\Omega t) + \text{c.c.} \tag{57}$$

in medium I, where $Q_{\mathrm{I}} = \alpha_{\mathrm{I}}/\varepsilon_{\mathrm{I}}$, and

$$H_{3z} = \tfrac{1}{2}\tau \exp[\mathrm{i}\alpha_3 (y - j\Lambda - l_2)] \exp(-\mathrm{i}\Omega t) + \text{c.c.} \tag{58}$$

$$E_{3x} = -\frac{1}{2}\frac{Q_3}{\varepsilon_0 \Omega} \tau \exp[\mathrm{i}\alpha_3 (y - j\Lambda - l_2)] \exp(-\mathrm{i}\Omega t) + \text{c.c.} \tag{59}$$

in medium 3, where $Q_3 = \alpha_3/\varepsilon_3$, ε_{I} and ε_3 are evaluated at $\Omega = 2\omega$. However, they are considered as constants, as in the previous section.

By using equation (33), the second harmonic magnetic and electric fields of the left interface in medium 2 of the zeroth cell are

$$H_{2z}^0 = \frac{1}{2}\left[U_l^0 \exp(\mathrm{i}\alpha_2 y) + V_l^0 \exp(-\mathrm{i}\alpha_2 y) + f_{1l}^0 \exp(\mathrm{i}\xi y) + f_{2l}^0 \exp(-\mathrm{i}\xi y) + f_{3l}^0\right] \times \exp(-\mathrm{i}\Omega t) + \text{c.c.} \tag{60}$$

$$E_{2x}^0 = \frac{1}{2}\frac{Q_2}{\varepsilon_0 \Omega}\left[-U_l^0 \exp(\mathrm{i}\alpha_2 y) + V_l^0 \exp(-\mathrm{i}\alpha_2 y)\right] \exp(-\mathrm{i}\Omega t) + \frac{1}{2}\frac{Q_{\mathrm{V}}}{\varepsilon_0 \Omega}\left[-f_{1l}^0 \exp(\mathrm{i}\xi y) + f_{2l}^0 \exp(-\mathrm{i}\xi y)\right] \exp(-\mathrm{i}\Omega t) + \text{c.c.} \tag{61}$$

and the second harmonic magnetic and electric fields of the right interface in medium 2 of the jth cell are

$$H_{2z}^{j} = \tfrac{1}{2}\big[U_r^j \exp[\mathrm{i}\alpha_2(y - j\Lambda - l_2)] + V_r^j \exp[-\mathrm{i}\alpha_2(y - j\Lambda - l_2)] + f_{1r}^j \exp[\mathrm{i}\xi(y - j\Lambda - l_2)] + f_{2r}^j \exp[-\mathrm{i}\xi(y - j\Lambda - l_2)] + f_{3r}^j\big] \times \exp(-\mathrm{i}\Omega t) + \text{c.c.} \tag{62}$$

$$E_{2x}^{j} = \frac{1}{2}\frac{Q_2}{\varepsilon_0\Omega}\left[-U_r^j \exp[\mathrm{i}\alpha_2(y - j\Lambda - l_2)] + V_r^j \exp[-\mathrm{i}\alpha_2(y - j\Lambda - l_2)]\right]\exp(-\mathrm{i}\Omega t) + \frac{1}{2}\frac{Q_{\mathrm{V}}}{\varepsilon_0\Omega}\left[-f_{1r}^j \exp[\mathrm{i}\xi(y - j\Lambda - l_2)] + f_{2r}^j \exp[-\mathrm{i}\xi(y - j\Lambda - l_2)]\right] \times \exp(-\mathrm{i}\Omega t) + \text{c.c.} \tag{63}$$

Applying boundary conditions at the $y = 0$ interface for the equation pairs (56), (60) and (57), (61), and at the $y = j\Lambda + l_2$ interface for the equation pairs (58), (62) and (59), (63), four boundary equations for second harmonic waves are obtained:

$$\rho = U_l^0 + V_l^0 + \phi_{hl}^0 \tag{64a}$$

$$Q_{\mathrm{I}}\rho = Q_2\left(-U_l^0 + V_l^0\right) + \phi_{el}^0 \tag{64b}$$

$$U_r^j + V_r^j + \phi_{hr}^j = \tau \tag{64c}$$

$$Q_2\left(-U_r^j + V_r^j\right) + \phi_{er}^j = -Q_3\tau \tag{64d}$$

where

$$\phi_{hl}^0 = f_{1l}^0 + f_{2l}^0 + f_{3l}^0 \tag{65a}$$

$$\phi_{el}^0 = Q_{\mathrm{V}}\left(-f_{1l}^0 + f_{2l}^0\right) \tag{65b}$$

$$\phi_{hr}^j = f_{1r}^j + f_{2r}^j + f_{3r}^j \tag{65c}$$

$$\phi_{er}^j = Q_{\mathrm{V}}\left(-f_{1r}^j + f_{2r}^j\right). \tag{65d}$$

From the second harmonic transfer matrix equations (52*a*)–(53), the complex amplitudes across j unit cells are related as

$$\begin{pmatrix} U_r^j \\ V_r^j \end{pmatrix} = F\begin{pmatrix} U_l^0 \\ V_l^0 \end{pmatrix} + G \tag{66a}$$

where

$$F = \Phi_4\Phi_9\Phi_2\,(\Delta)^{j-1}\,\Phi_{11}\Phi_4 \tag{66b}$$

$$G = \Phi_4\Phi_9\Phi_2\,(\Delta)^{j-1}\,\Phi_{12}^0 + \Phi_4\Phi_9\Phi_2\sum_{r=1}^{j-1}(\Delta)^{j-1-r}\,\Upsilon^r + \Phi_4\Phi_{10}^j. \tag{66c}$$

Expanding (66*a*), we obtain

$$U_r^j = F_{11}U_l^0 + F_{12}V_l^0 + G_{11} \tag{67a}$$

$$V_r^j = F_{21}U_l^0 + F_{22}V_l^0 + G_{21}. \tag{67b}$$

The substitution of equations (67*a*) and (67*b*) into the boundary equations (64*a*)–(64*d*) gives the second harmonic reflection and transmission coefficients ρ and τ as

$$\rho = U_l^0 + V_l^0 + \phi_{hl}^0 \tag{68}$$

$$\tau = (F_{11} + F_{21})\,U_l^0 + (F_{12} + F_{22})\,V_l^0 + G_{11} + G_{21} + \phi_{hr}^j \tag{69}$$

where

$$U_l^0 = \frac{O_{22}C_{11} - O_{12}C_{21}}{O_{11}O_{22} - O_{12}O_{21}} \tag{70}$$

$$V_l^0 = \frac{-O_{21}C_{11} + O_{11}C_{21}}{O_{11}O_{22} - O_{12}O_{21}} \tag{71}$$

and

$$O_{11} = (Q_{\mathrm{I}} + Q_2) \tag{72a}$$

$$O_{12} = (Q_{\mathrm{I}} - Q_2) \tag{72b}$$

$$O_{21} = Q_2 (F_{21} - F_{11}) + Q_3 (F_{11} + F_{21}) \tag{72c}$$

$$O_{22} = Q_2 (F_{22} - F_{12}) + Q_3 (F_{12} + F_{22}) \tag{72d}$$

$$C_{11} = \phi^0_{el} - Q_{\mathrm{I}} \phi^0_{hl} \tag{72e}$$

$$C_{21} = -Q_2 (G_{21} - G_{11}) - \phi^j_{er} - Q_3 \left(G_{11} + G_{21} + \phi^j_{hr} \right). \tag{72f}$$

Calculations of Poynting's vector in medium I and medium 3 show that the second harmonic transmission and reflection coefficients through the entire multilayers are

$$T_{\mathrm{SHG}} = \frac{\varepsilon_1}{\varepsilon_3} \frac{|\tau|^2}{|p|^2} \qquad \text{and} \qquad R_{\mathrm{SHG}} = \frac{|\rho|^2}{|p|^2} \tag{73}$$

where ε_{I} and ε_3 are the dielectric constants for medium I and medium 3 that sandwich the multilayer.

3. Results and discussion

The calculated results of equations (30) for linear transmission and reflection coefficients, and equations (73) for second harmonic transmission and reflection coefficients, have been applied by using the macroscopic parameters of FeF_2 for the antiferromagnetic slabs and ZnF_2 for the dielectric slabs. FeF_2 is a uniaxial two-sublattice antiferromagnet with a dielectric constant $\varepsilon_2 = 5.5$, a gyromagnetic ratio $\gamma/\mu_0 = 1.05$ cm^{-1} T^{-1}, an exchange field $\mu_0 H_E = 53.3$ T, an anisotropy field $\mu_0 H_A = 19.7$ T, a sublattice magnetization $\mu_0 M_0 = 0.056$ T and an applied static magnetic field in the direction of the z-axis $\mu_0 H_0$, whereas ZnF_2 is assumed to be a simple dielectric with a dielectric constant $\varepsilon_1 = 8.0$.

In the calculations, the chosen multilayers consist of 7 and 12 complete unit cells. As a whole, there are 8 FeF_2 slabs and 7 ZnF_2 slabs in the multilayer with 7 complete unit cells, and 13 FeF_2 slabs and 12 ZnF_2 slabs in the multilayer with 12 complete unit cells. The chosen damping parameter is $\eta = 5 \times 10^{-4}$ [14], and the applied static field is $\mu_0 H_0 = 3$ T parallel to the slabs. With these damping parameters and applied static field, the second harmonic susceptibility elements are significant in the vicinities and at the antiferromagnetic resonances, 49.3 and 55.6 cm^{-1} [13, 14], where the linear absorption is significant. This is the range where the second harmonic waves are expected. Away from these resonances, the second harmonic susceptibility elements are effectively zero. Since the calculation involves the second harmonic effect in multilayers, the numerical errors have to be taken care of in the numerical evaluation of equations (30) and (73). This is done by checking the energy conservation, or the total energies of linear and second harmonic transmissions, and reflections should be less than or equal to the incident energy, I_p. In the region far away from the antiferromagnetic resonance, any peaks in the calculated spectra, whether the energy is conserved or not, should be considered as a numerical error because the second harmonic susceptibility elements are zero. If the experimentalists observe any second harmonic signal far away from the antiferromagnetic resonance, these must be due to some other effects where further theory is required to explain their appearance.

The linear transmission and reflection coefficients are plotted versus a wide range of frequency sweep in order to exhibit the features of the multilayer film. The thicknesses of ZnF_2 and FeF_2 slabs are fixed as $l_1 = 20$ μm and $l_2 = 40$ μm respectively. With all these parameters, the calculated linear reflection and transmission coefficients are shown in figure 3,

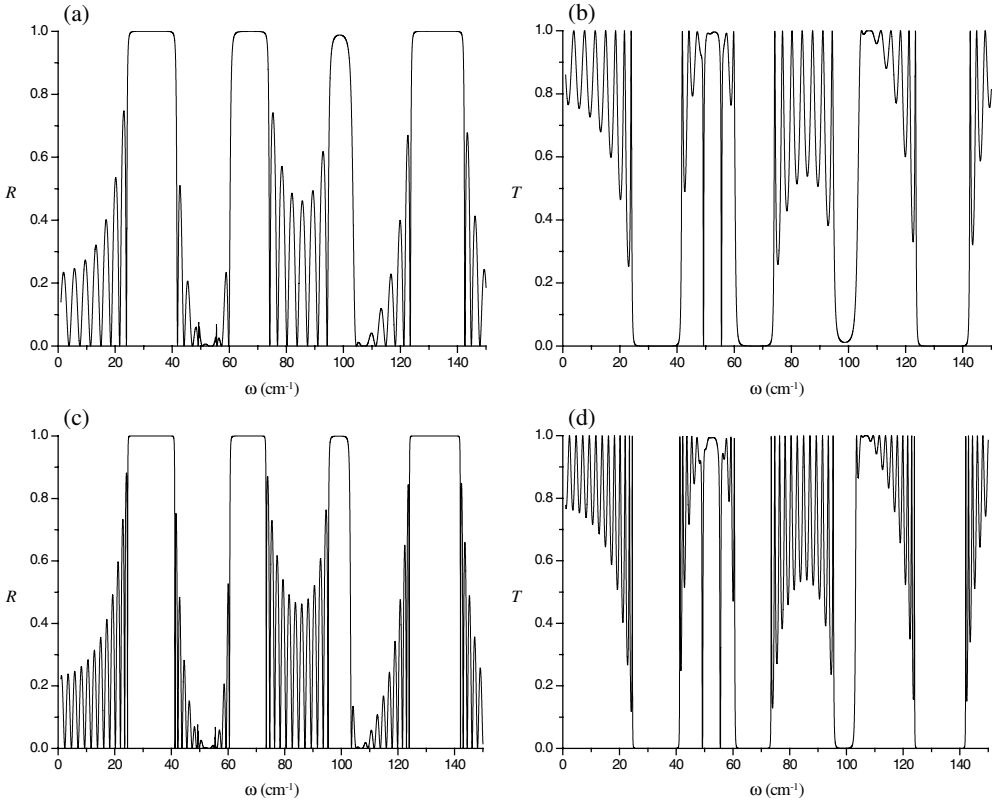

Figure 3. Linear reflection and transmission of FeF_2/ZnF_2 multilayers versus frequency sweep with thicknesses for ZnF_2 slabs, $l_1 = 20\ \mu$m, and FeF_2 slabs, $l_2 = 40\ \mu$m, in 3 T applied magnetic field: (a) linear reflection for $j = 7$; (b) linear transmission for $j = 7$; (c) linear reflection for $j = 12$; (d) linear transmission for $j = 12$.

and the corresponding second harmonic reflection and transmission coefficients are shown in figure 4 versus frequency sweep. The input intensity to produce the results in figures 3 and 4 is $I_p = 1.6 \times 10^{15}$ W m^{-2} [14].

From figures 3(a) to (d), the linear reflection and transmission curves show clearly the typical stop bands of superlattice structures, with reflection close to unity and transmission close to zero [5, 6]. The location and the width of the stop bands are due to the periodic structure of the multilayers, which introduces the gaps in the energy bands depending on the wavevector, k_V, k_1 and the thicknesses of the slabs, l_1 and l_2 [1, 5, 6]. This feature is more obvious in figures 3(c) and (d) with more complete unit cells. The antiferromagnetic resonance dips expected at 49.3 and 55.6 cm^{-1} for 3 T of applied static field [14] intervene with the fringes of spatial resonances and the stop band. The dips at the resonances for both transmission and reflection curves are due to the strong antiferromagnetic absorption in the vicinity and at the antiferromagnetic resonance frequencies, whereas the fringes outside the stop bands and away from antiferromagnetic resonances are due to the dimensional resonance in the periodic structure depending on the wavevector, k_V, k_1 and the thicknesses of the slabs, l_1 and l_2.

The second harmonic reflection and transmission are about three orders weaker than the linear transmission and reflection, and are significant in the vicinity and at the antiferromagnetic resonances. These are shown in figures 4(a)–(d). From the curves shown in figures 4,

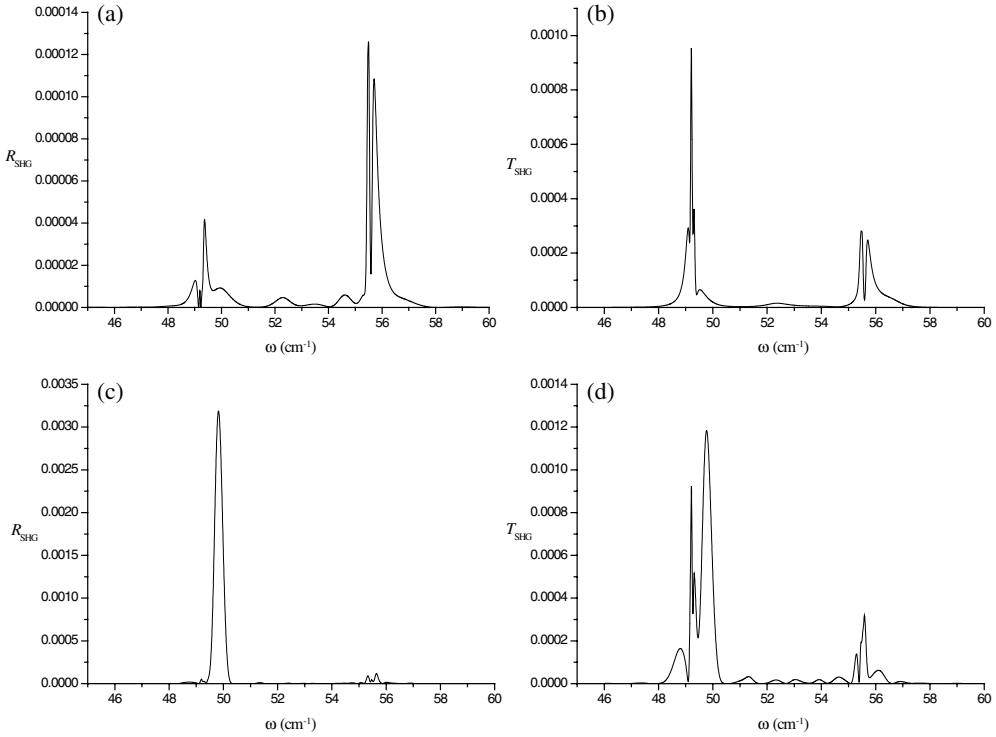

Figure 4. Second harmonic (SH) reflection and transmission of FeF_2/ZnF_2 multilayers versus frequency sweep with thicknesses for ZnF_2 slabs, $l_1 = 20$ μm, and FeF_2 slabs, $l_2 = 40$ μm in 3 T applied magnetic field: (a) SH reflection for $j = 7$; (b) SH transmission for $j = 7$; (c) SH reflection for $j = 12$; (d) SH transmission for $j = 12$.

it is obvious that the main second harmonic transmission and reflection peaks at the antiferromagnetic resonances are sharpened by the multilayer structure as compared with the previous calculation for a single FeF_2 film [14]. The present result also shows that the minor fringes away antiferromagnetic resonances of a single FeF_2 film are drastically reduced when FeF_2 is structured in a multilayer with an interleaving dielectric, in comparison to what has been calculated for an isolated FeF_2 slab [14]. The other important feature is the multilayer structure enhances the phase difference between the generated second harmonic transmission and reflection waves. This is obvious if we compare the shapes of the spectra in figures 4(a) and (b) for 7 complete unit cells, and figures 4(c) and (d) for 12 complete unit cells. Moreover, for all spectra shown in figure 4, the magnitudes and patterns of the peaks are different at the two antiferromagnetic resonances. This feature differs from the previous results for a single FeF_2 film [14], where the magnitudes and patterns of the peaks are almost the same at the two antiferromagnetic resonances.

4. Conclusion

The main result of this paper is the calculation and formulation of the second harmonic waves generated through an antiferromagnetic/dielectric multilayer based entirely on the transfer matrix formalism and the nonlinear magnetic response of an antiferromagnet. The calculations are a combination of transfer matrix technique and conventional nonlinear optics approach

with the assumption of no depletion of the input waves and without the assumption of slowly varying enveloped approximation, where about 0.1% of the input intensity is converted to second harmonic waves at the antiferromagnetic resonances. The calculated spectra show several distinctive features as compared to the previous results of a single FeF_2 film [14]. Namely, the presence of stop bands in the linear spectra, the sharpened main peaks of second harmonic spectra at antiferromagnetic resonances, and the fact that minor peaks away from resonances are almost disappeared, and the obvious phase difference between transmission and reflection spectra, and between the main peaks at two antiferromagnetic resonances in all spectra. The methodology shown in this paper is a preliminary study on the nonlinear waves in antiferromagnetic/dielectric multilayers, and will facilitate the future studies on more general cases, such as second harmonic generation with depletion of the input waves for ferromagnetic/dielectric systems where the assumption of weak nonlinearity cannot be used.

Acknowledgment

This study was supported by a research grant provided by Universiti Sains Malaysia, Penang, Malaysia.

References

[1] Raj N and Tilley D R 1989 The electrodynamics of superlattices *The Dielectric Function of Condensed Systems* ed L V Keldysh, D A Kirzhnitz and A A Maradudin (Amsterdam: Elsevier) chapter 7
[2] Hazidad R, Tilley D R and Tilley J 1991 *J. Phys.: Condens. Matter* **3** 291–8
[3] Dumelow T, Parker T J, Smith S R P and Tilley D R 1993 *Surf. Sci. Rep.* **17** 151–212
[4] Abraha K and Tilley D R 1996 *Surf. Sci. Rep.* **24** 125–222
[5] Wang J J, Zhou X F, Wan W L, Wang X Z and Tilley D R 1999 *J. Phys.: Condens. Matter* **11** 2697–705
[6] Zhou X F, Wang J J, Wang X Z and Tilley D R 2000 *J. Magn. Magn. Mater.* **212** 82–90
[7] Albuquerque E L and Cottam M G 2003 *Phys. Rep.* **376** 225–337
[8] Gao H, Wang X Z and Xu X R 2003 *J. Magn. Magn. Mater.* **257** 151–7
[9] Huang K, Kahn L M and Mills D L 1990 *Phys. Rev.* B **41** 7981–7
[10] Hashizume N, Ohashi M, Kondo T and Ito R 1995 *J. Opt. Soc. Am.* B **12** 1894–904
[11] Wu Y Z, Vollmer R, Regensburger H, Jin X F and Kirschner J 2000 *Phys. Rev.* B **63** 054401
[12] Wang X Z and Fu S F 2004 *J. Magn. Magn. Mater.* **271** 334–47
[13] Lim S C, Osman J and Tilley D R 2000 *J. Phys. D: Appl. Phys.* **33** 2899–910
[14] Lim S C 2002 *J. Opt. Soc. Am.* B **19** 1401–10
[15] Butcher P N and Cotter D 1990 *The Elements of Nonlinear Optics* (Cambridge: Cambridge University Press) pp 5, 211–226
[16] Mills D L 1998 *Nonlinear Optics* 2nd edn (New York: Springer) p 5